whose only impact on the electric field is a global reversal of its direction, should not alter the relative spacing of field lines in a CFLD. Since the sign-reversed version of Fig. 6 must show uniform spacing of the outgoing field lines on the +4 charge, equatorial clumping does not show the invariance under charge reversal that would be expected of a true field property.

[9]Phillip M. Rinard, Delbert Brandley, and Keith Pennebaker, "Plotting Field Intensity and Equipotential Lines," Am. J. Phys. **42**, 792–793 (1974).

[10]While charge distributions lacking a monopole moment possess divergent field lines, such as the $\theta=0$ and $\theta=\pi$ lines in the dipole, such lines are few in number and can be avoided by the proper choice of θ_0. By contrast, the number of divergent lines associated with a false monopole moment is proportional to N, and is unaffected by the choice of θ_0. In several figures, including the dipole CFLD of Fig. 1(a), gaps on negative charges were avoided by setting θ_0 to a value very close to 0, producing an apparently divergent field line that eventually reappears at the opposite end of the diagram and terminates on a negative charge.

[11]Edwin A. Abbot, *Flatland: A Romance of Many Dimensions by a Square* (Seeley & Co., London, 1884). For a more technical discussion of two-dimensional science, see A. K. Dewdney, *The Planiverse: Computer Contact with a Two-dimensional World* (Poseidon, New York, 1984). While this article was in press, the authors were made aware of the recent note of T. E. Freeman, "One-, two-, or three-dimensional fields?," Am. J. Phys. **63**, 273–274 (1995). Freeman shows a field line diagram with a false monopole moment and correctly observes that the distortion would disappear in a two-dimensional universe.

[12]Boundary clumping can be avoided in a distribution with one negative and several positive charges by reversing the sign of each charge. A form of boundary clumping can be seen in charge distributions containing a single positive charge, but the problem originates solely from numerical errors that are easily avoided.

[13]The problem of distributing points uniformly on a sphere is discussed in the Internet document sphere.faq, produced by Dave Rusin. The document is located at: http://www.math.niu.edu:80/~rusin/papers/spheres/sphere.faq. Uniform tilings are not achieved on golf balls or geodesic domes which either employ multiple tiling elements or contain defects at the north pole or at the equatorial "weld" line.

[14]Reference 13 describes methods of obtaining nearly uniform distributions of an arbitrary number of points on the surface of a sphere.

[15]If field line diagrams are seen as primarily serving visualization and pedagogic purposes (rather than serving as a practical research/design tool) it may be time to reevaluate their pedagogic worth. Tornkvist *et al.* suggest that, independent of any imperfections that may be present in CFLDS, students often misinterpret these diagrams. S. Tornkvist, A. Petterson, and G. Transtromer, "Confusion by representation: On students' comprehension of the electric field concept," Am. J. Phys. **61**, 335–338 (1993).

Resonant Faraday rotation as a probe of atomic dispersion

D. A. Van Baak
Department of Physics, Calvin College, Grand Rapids, Michigan 49546

(Received 18 August 1995; accepted 4 December 1995)

The Faraday effect (the rotation of the plane of polarization of light as it propagates through a sample parallel to a static magnetic field) is readily detected in room-temperature rubidium vapor by a diode-laser experiment near the D_2 resonance line at 780 nm, and the theoretical treatment of this effect provides an unusually clear insight into the relation between absorption and dispersion in the interaction of light with matter. © *1996 American Association of Physics Teachers.*

I. INTRODUCTION

Impelled by a belief in the unity of the forces of nature, Michael Faraday sought, and in 1845 provided, the first phenomenological evidence for a connection between light and magnetism when he discovered the effect that still bears his name. He found that plane-polarized light, propagating through matter parallel to a static magnetic field, underwent a systematic rotation of its plane of polarization. The effect, though unambiguous, is typically not large, with rotation per unit distance per unit field of order 10 rad/m T ($\approx$0.03 arcmin/cm Oe) in ordinary glass samples in the midvisible; this "Verdet constant" is itself a function of wavelength, typically growing dramatically toward the blue end of the visible spectrum. Not until the atomic-electron hypothesis toward the end of the 19th century was it possible to provide a more detailed model for Faraday rotation; Becquerel predicted a Verdet constant related to the dispersion $dn/d\lambda$ of the material. A modern picture of Faraday rotation emerges from the quantum-mechanical response of an atom to a magnetic field; in this picture the atomic absorption and dispersion are both affected by the field, and in this sense the Faraday effect is to dispersion what the Zeeman effect is to absorption (or emission).

Given the small magnitude of Faraday rotation in bulk condensed matter, it might seem impossible to detect the effect for a much more dilute gas sample. It is the connection between absorption and dispersion that contradicts this expectation; both effects are subject to enormous enhancements near atomic resonances. This paper will work out the theory of Faraday rotation for light interacting with a simple model system, and will derive the behavior of the Verdet constant both far from, and very near, an atomic resonance. The calculation, in turn, is motivated by the possibility of observing resonant Faraday rotation in an atomic vapor, in this case by the interaction of 780 nm diode-laser radiation with a room-temperature sample of rubidium vapor. The notable and detailed agreement between observed rotation signals, and those computed from a theory involving atomic dispersion, demonstrates the reality of dispersion, and its intimate connection with absorption. Since the absorption and fluorescence of rubidium vapor under diode-laser excitation is an

emerging classic experiment in diode-laser optics, and since only very modest extra equipment is needed to display Faraday rotation, a growing number of students will be able to appreciate directly this probe of the dispersion that always accompanies atomic absorption.

Faraday's own account of his discovery is available in a reprint edition;[1] discussions of it in biographical[2] and bibliographical[3] contexts are also available. The enhancement of the Faraday effect near resonance lines in atomic vapors was discovered in 1898 by Macaluso and Corbino[4] and has been applied in modern times to create narrow-band optical filters.[5] Two earlier papers in this Journal describe Faraday-rotation experiments in bulk matter;[6,7] this effect has also become the basis of optical isolators.[8] The derivation worked out in this paper has been guided by that of Preston and Dietz,[9] who however are motivated by experiments on nonresonant rotation in bulk matter.

Section II of this paper gives a quantum-mechanical treatment of Faraday rotation in a dilute vapor of a model atomic system. Section III discusses the instrumental requirements for diode-laser spectroscopy of rubidium vapor in general, and the added requirements for Faraday-rotation experiments in particular. Section IV presents and discusses typical experimental results, and Sec. V presents conclusions and applications.

II. THEORY

We divide this derivation of Faraday rotation into four parts. The first step is to consider the propagation of linearly polarized light through a medium, resolving it into two oppositely directed circularly polarized fields which are assumed to propagate independently. The second step is to relate the macroscopic index of refraction, and the attenuation, of the two circular polarization components in a medium to the microscopic susceptibility of the atoms in the sample. The third step introduces the simplest quantum-mechanical system for which the susceptibility can be computed, and extracts the results for Faraday rotation. Finally this section takes up the effects of Doppler broadening on the signals computed from the model.

The first step of the theory resembles Fresnel's method for understanding optical rotation in chiral media, in which an incident linearly polarized field is decomposed into two oppositely directed circularly polarized fields of equal amplitude; the fundamental assumption is that each circularly polarized field propagates independently (but differently) through the medium. Here we will suppose that each of the two circular polarizations has its own index of refraction and attenuation coefficient, and work out the results for propagation.

We introduce the two circularly polarized fields[10] propagating in the $+\mathbf{z}$ direction (real parts understood):

$$\mathbf{E}_{\pm}(z,t)=E_0(\hat{\mathbf{x}}\pm i\hat{\mathbf{y}})\ \exp\, i(kz-\omega t) \tag{1}$$

and write the incident field as the superposition

$$\mathbf{E}(0,t)=\mathbf{E}_{+}(0,t)+\mathbf{E}_{-}(0,t)=2E_0\ \hat{\mathbf{x}}\ \exp\, i(k0-\omega t), \tag{2}$$

which is clearly a linearly polarized field with polarization along $\mathbf{x}$. Now we assume that the fields $\mathbf{E}_{\pm}$ propagate with indices of refraction $n_{\pm}$ and attenuation constants $\beta_{\pm}$ respectively. Then the wave number k is given by

$$k_{\pm}=\frac{2\pi}{\lambda/n_{\pm}}=\frac{2\pi}{\lambda}\,n_{\pm}, \tag{3}$$

where λ is the *vacuum* wavelength of the light, and the incident field propagates through a sample of length L to give the emergent field

$$\mathbf{E}(L,t)=E_0\ \exp(-\beta_{+}L)(\hat{\mathbf{x}}+i\hat{\mathbf{y}})\exp\, i\left(\frac{2\pi}{\lambda}\,n_{+}L-\omega t\right)$$
$$+E_0\ \exp(-\beta_{-}L)(\hat{\mathbf{x}}-i\hat{\mathbf{y}})\exp\, i\left(\frac{2\pi}{\lambda}\,n_{-}L-\omega t\right). \tag{4}$$

In the usual case of equal attenuations for the two polarizations ($\beta_{+}=\beta_{-}=\beta$), this reduces to

$$\mathbf{E}(L,t)=2E_0\ \exp(-\beta L)(\hat{\mathbf{x}}\cos\Delta\theta-\hat{\mathbf{y}}\sin\Delta\theta)$$
$$\times\exp\, i\left(\frac{2\pi}{\lambda}\,\frac{n_{+}+n_{-}}{2}\,L-\omega t\right), \tag{5}$$

which clearly represents a linearly polarized wave whose direction of polarization has been rotated through the Faraday rotation angle $\Delta\theta$, given by

$$\Delta\theta=\frac{2\pi}{\lambda}\left(\frac{n_{+}-n_{-}}{2}\right)L. \tag{6}$$

In Sec. III we will see how this rotation signal $\Delta\theta$ can be extracted from (4) even when differential attenuation is present.

The second stage of the theoretical derivation is to relate the macroscopic parameters n and β to the microscopic behavior of the sample. This can be achieved by assuming that the medium as a whole develops, in response to the electric field $\mathbf{E}$, an electric polarization $\mathbf{P}$ given by

$$\mathbf{P}=\epsilon_0\chi\mathbf{E}, \tag{7}$$

where for a dilute-gas sample we do not need to distinguish between the incident and the "local" value of the electric field. The electric susceptibility χ defined by (7) is a dimensionless, complex, and frequency-dependent scalar quantity characterizing the sample. Under this assumption, Maxwell's equations give the relationship between wave number k and frequency ω for any monochromatic plane wave propagating through the material:

$$\left(\frac{kc}{\omega}\right)^2=1+\chi. \tag{8}$$

In the limit of low density, we will see that $|\chi|$ is so small even near resonance that we can adequately write

$$\frac{kc}{\omega}=1+\frac{\chi}{2}; \tag{9}$$

then the usual decomposition of χ into real and imaginary parts

$$\chi=\chi'+i\chi'' \tag{10}$$

gives the results

$$n=1+\frac{\chi'}{2}\quad\text{and}\quad\beta=\frac{2\pi}{\lambda}\,\frac{\chi''}{2}. \tag{11}$$

Thus the macroscopic propagation constants n and β have been related to the real and imaginary parts of the microscopic susceptibility, respectively.

The third part of the derivation is to assume a model for the medium and to compute its electric susceptibility. The

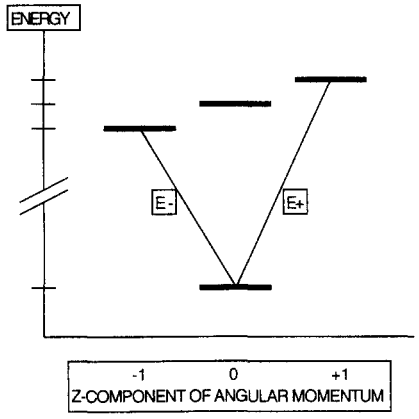

Fig. 1. The model atomic system used in this paper to compute absorption, dispersion, and Faraday rotation in a dilute vapor. The ground state is nondegenerate, and the excited state has three magnetic sublevels, here shown as slightly split by an external magnetic field.

simplest model system is a gas of independent atoms, of number density N, with each atom having a nondegenerate ground state and an excited state forming a Zeeman triplet, as shown in Fig. 1. This is exemplified by a ${}^1S_0-{}^1P_1$ transition of an atom with no nuclear spin or hyperfine structure; such an atom shows the "normal" Zeeman effect, and in the presence of a magnetic field $\mathbf{B}=B\hat{\mathbf{z}}$ the upper-state sublevels split as shown in Fig. 1, with $m=\pm 1$ states undergoing energy shift

$$\Delta E=\pm\mu_B B, \tag{12}$$

where $\mu_B=e\hbar/2m_e$ is the Bohr magneton. Then transitions from the (unshifted) ground state to the $m=\pm 1$ excited states will occur at Bohr frequencies

$$\nu_{0\pm}=\nu_0+\frac{\Delta E}{h}=\nu_0\pm\frac{\mu_B B}{h}=\nu_0\pm\frac{e}{4\pi m_e}B. \tag{13}$$

For the electric fields introduced in (1), the electric-dipole selection rules allow the fields $\mathbf{E}_\pm$ to induce only the resonant upward transitions with $\Delta m=\pm 1$ respectively. Thus each circular polarization will separately interact with its own two-level system, and so each polarization will propagate with its own index of refraction and attenuation constant, as was assumed above. These numbers, in turn, will be those arising from the susceptibility of a generic two-level atomic system, which is given as a function of optical frequency ν by[11]

$$\chi(\nu)=\frac{N\lambda^3}{16\pi^3\tau}\frac{1}{\nu_0-\nu-i\Delta\nu/2}, \tag{14}$$

where $\lambda=c/\nu$, ν_0 is the Bohr frequency of the transition, $\Delta\nu=(2\pi\tau)^{-1}$ is its "natural linewidth" (full-width at half-maximum, in ordinary frequency), and τ is the spontaneous-decay lifetime of the upper state.

Then from the result (11) above, we can write the attenuation constant for the electric field as

$$\beta(\nu)=\frac{N\lambda^2}{16\pi^2\tau}\frac{\Delta\nu/2}{(\nu-\nu_0)^2+(\Delta\nu/2)^2}, \tag{15}$$

which shows the conventional Lorentzian line shape. It gives peak absorption at line center, where $\nu=\nu_0$ and $\lambda=\lambda_0=c/\nu_0$; here β reaches the value

$$\beta_{\max}=\frac{N\lambda_0^2}{16\pi^2\tau}\frac{2}{\Delta\nu}=\frac{N\lambda_0^2}{4\pi}. \tag{16}$$

Again from the earlier result (11), we can deduce for the index of refraction $n(\nu)$ of the sample the curve

$$n(\nu)-1=\frac{N\lambda^3}{32\pi^3\tau}\frac{\nu_0-\nu}{(\nu-\nu_0)^2+(\Delta\nu/2)^2}, \tag{17}$$

which shows a dispersive dependence on frequency, with positive values occurring below the resonant frequency, and a peak departure of index n from unity occurring at frequencies $\nu=\nu_0\pm\Delta\nu/2$, of size

$$|n-1|_{\max}=\frac{N\lambda_0^3}{32\pi^3\tau}\frac{1}{\Delta\nu}=\frac{N\lambda_0^3}{16\pi^2}=\beta_{\max}\frac{\lambda_0}{4\pi}. \tag{18}$$

This tightly related behavior of absorption and dispersion has distinct implications for an experiment seeking to detect atomic dispersion; for example, if a sample of length L is dense enough to attenuate, at line center, the fields to e^{-1} (or the transmitted power to $e^{-2}=13.5\%$), then it has $\beta_{\max}L=1$, so

$$|n-1|_{\max}=\frac{\lambda_0}{4\pi L}, \tag{19}$$

which is very small indeed for plausible sample lengths. If one tries to detect this deviation of refractive index from unity by interferometric means, then the phase shift (relative to vacuum) that will accumulate in a one-way trip through this sample is

$$\Delta\phi=\frac{2\pi}{\lambda}|n-1|L, \quad \text{so } \Delta\phi_{\max}=\frac{2\pi}{\lambda_0}\frac{\lambda_0}{4\pi L}L=\frac{1}{2}\text{ (radian)}. \tag{20}$$

This phase shift is only 8% of the 2π radians required to produce a single interferometric fringe, and it would have to be detected in the face of the deep absorption accompanying it. Conventional detection of atomic dispersion is carried out much farther from line center, using samples of much greater optical thickness, and relying on the fact that dispersion drops off with detuning less rapidly than does absorption. We will see that Faraday rotation offers an indirect, but vastly easier, way to detect atomic dispersion, even for optically thin samples, and that the Faraday rotation signal can be followed right through resonance.

The absorption and dispersion signals thus far computed are shown in Fig. 2, in which axes have been normalized to "natural" values. The horizontal axis gives frequency in units of the natural linewidth $\Delta\nu$, so that the absorption signal reaches half-maximum, and the dispersion signal reaches its extrema, at ordinate $\pm 1/2$. The dispersion-shaped signal gives $n(\nu)-1$ in the units shown; for reference, the room-temperature number density of rubidium[12] is near $N=2.5\times10^{16}$ m^{-3}, so that at a resonant wavelength of $\lambda_0=0.78\times10^{-6}$ m, the factor $N\lambda_0^3/8\pi^2$ has value 15×10^{-5}. This means the computed index of refraction is confined to the range $1\pm(75\times10^{-6})$, and it shows that the $|\chi|\ll 1$ assumption made above is retrospectively justified.

With all these preliminaries, we can now calculate the Faraday rotation signal and its frequency dependence. Given the separate resonant frequencies (13) for the oppositely directed circularly polarized fields $\mathbf{E}_\pm$, we can form the difference of refractive indices called for in (6), and write

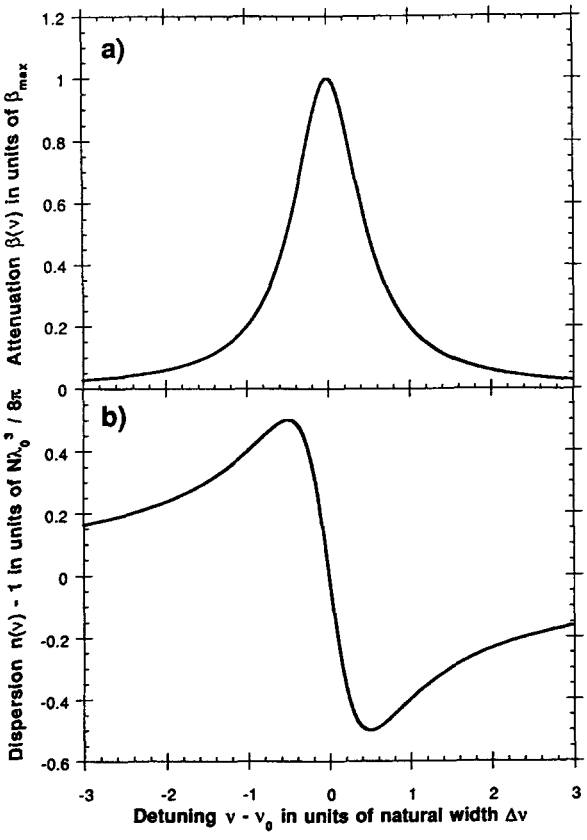

Fig. 2. Graphs of the absorption (a) and dispersion (b) signals computed for the model two-level atomic system, in the absence of Doppler broadening. The curves arise from Eqs. (15) and (17) respectively; the horizontal scale is in units of the "natural linewidth" $\Delta\nu$, and the vertical scales are in units natural to the problem.

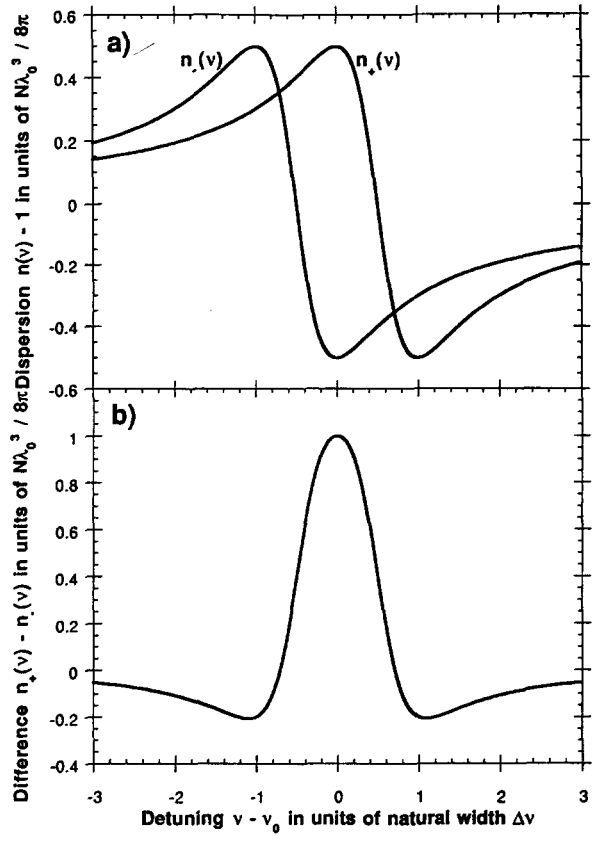

Fig. 3. (a) Dispersion curves for the two circular polarizations of light in the Zeeman-split model atomic system in the absence of Doppler broadening, computed for the particular choice of magnetic field strength $(e/4\pi m_e)B=\Delta\nu/2$. (b) The Faraday-rotation angle computed from the curves in (a), showing the characteristic symmetric signal predicted for resonant Faraday rotation.

$$\Delta\theta(\nu)=\frac{N\lambda^2 L}{32\pi^2\tau}\left[\frac{\nu_{0+}-\nu}{(\nu_{0+}-\nu)^2+(\Delta\nu/2)^2}-\frac{\nu_{0-}-\nu}{(\nu_{0-}-\nu)^2+(\Delta\nu/2)^2}\right]. \tag{21}$$

Figure 3 shows the general character of the Faraday rotation signal deduced from this result; its frequency dependence arises from the difference of two (offset) dispersion signals, so that the $\Delta\theta(\nu)$ signal has a symmetric form, centered at the unshifted line center ν_0. The analytic form of the Faraday rotation signal is thus a bit complicated, but two special cases are worth extracting.

The first is applicable whenever the magnetic field (and thus the Zeeman shift) is small enough; it makes use of the general result

$$f(x+\epsilon)-f(x-\epsilon)=2\epsilon\, f'(x)+O(\epsilon^3), \tag{22}$$

which [using (17)] allows (21) to be written (to lowest order in B) as

$$\Delta\theta=VBL, \quad \text{with } V=\frac{1}{\lambda}\frac{e}{2m_e}\frac{dn}{d\nu}=-\frac{e}{2m_e c}\,\nu\,\frac{dn}{d\nu}. \tag{23}$$

Thus the Faraday rotation $\Delta\theta$ is predicted to be proportional to the strength of the magnetic field and the sample length, with a proportionality factor V called the Verdet constant; and V is predicted to have a frequency dependence $-\nu\, dn/d\nu$, or $\lambda\, dn/d\lambda$, in agreement with the Becquerel formula.[13]

Actual materials with electronic structure much more complicated than that modelled here do in fact follow the Becquerel form of V quite closely, except for a multiplicative correction factor (the magneto-optic constant γ) generally somewhat smaller than unity.[14] It is worth noting that the wavelength dependence of Faraday rotation is given by the dimensionless quantity $\lambda\, dn/d\lambda$, and that its scale is fixed by the combination of fundamental constants

$$\frac{e}{2m_e c}=293.34 \text{ rad/T m}=1.0084 \text{ arcmin/Oe cm}. \tag{24}$$

These results for small field B also make it clear why Faraday rotation can be so enormously enhanced near an atomic resonance. First, the index of refraction n departs maximally from unity near a resonance, and second, it does so with a dispersive shape, going from maximum to minimum in a frequency span of only the natural linewidth. Thus a quotient like $\Delta n/\Delta\nu$ has, near resonance, the largest possible numerator and a very small denominator. In terms of the graph of Fig. 3(a), ordinary nonresonant Faraday rotation depends on a tiny difference between two refractive indices, each of which is separately very close to one; but resonant Faraday rotation involves the difference of two refractive indices, each of which is near its maximum possible departure from unity, and whose departures from unity are of *opposite sign.*

This enhancement of Faraday rotation at a resonance motivates the examination of a second special case of (21), namely, the Faraday rotation at the center of the (zero-field) atomic resonance, at $\nu=\nu_0$. The result is

$$\Delta\theta|_{\nu=\nu_0}=\frac{N\lambda_0^2 L}{32\pi^2\tau}\,2\,\frac{kB}{(kB)^2+(\Delta\nu/2)^2}, \tag{25}$$

where $k=e/4\pi m_e=13.996$ GHz/T; this function grows linearly with B (for $kB\ll\Delta\nu/2$), reaches a maximum at $kB=\Delta\nu/2$, and then decreases gradually. The initial linear dependence of Faraday rotation on B allows the extraction of an at-resonance Verdet constant of

$$V_{\rm res}=\frac{1}{L}\left.\frac{d(\Delta\theta)}{dB}\right|_{B=0}=\frac{N\lambda_0^2}{32\pi^2\tau}\,2\,\frac{k}{(\Delta\nu/2)^2}=\frac{N\lambda_0^2}{4\pi}\,\frac{e}{m_e}\,\tau, \tag{26}$$

which for values of experimental interest like $N=2.5\times10^{16}$ $\rm m^{-3}$, $\lambda_0=0.78\times10^{-6}$ m, $e/m_e=1.76\times10^{11}$ C/kg, and $\tau=25.5\times10^{-9}$ s (Ref. 15) yields the enormous value of $V=5.4\times10^{6}$ rad/T m. Thus despite a gas density some 12 orders of magnitude smaller than that of typical solids, the resonant Faraday effect yields a computed Verdet constant about 5 orders of magnitude larger than that seen in bulk matter!

The maximum value of Faraday rotation at $kB=\Delta\nu/2$ in (25) arises from the particular circumstance depicted in Fig. 3(a), where the dispersion curves for n_+ and n_- are split apart by the Zeeman effect until the maximum of one lies immediately above the minimum of the other; this maximizes the difference n_+-n_- and thus the Faraday rotation. The maximum value of the rotation angle is given by

$$\Delta\theta_{\max}=\frac{N\lambda_0^2 L}{32\pi^2\tau}\,\frac{2}{\Delta\nu}=\frac{N\lambda_0^2 L}{8\pi}. \tag{27}$$

If we again suppose that the sample density and length have been chosen so as to attenuate transmitted light by factor e^{-2} at resonance (when the magnetic field is off), then the relation $\beta_{\max}L=1$ again applies, and from (16) the maximum Faraday rotation obtainable with this sample is

$$\Delta\theta_{\max}=\frac{N\lambda_0^2 L}{8\pi}=\frac{4\pi}{8\pi}=\frac{1}{2}\ \text{(radian)}. \tag{28}$$

Once again, the intimate relationship between absorption and dispersion has imposed a maximum on the signal obtainable with a sample of a given optical thickness, and once again the observable signal is limited to one-half radian. But this Faraday rotation of 0.5 rad is vastly easier to detect experimentally than the 0.5 rad of phase shift derived in (20) above. First, no interferometric setup is required to obtain the Faraday-rotation signal, but rather the mere one-way transmission of linearly polarized light through a sample; second, the signal to be extracted is not the phase shift of a fringe pattern, but the much more concrete rotation in space of the plane of polarization of the transmitted light.

The absorption, dispersion, and Faraday-rotation signals computed thus far are complicated, in experimental practice, by the Doppler effect. Rather than a sample of atoms all at rest and all sharing a common resonant frequency ν_0 (or its Zeeman-shifted equivalent), the experimenter confronts a sample of atoms of mass m, sharing common rest frequency ν_{00}, but spread out in velocity component v_z according to the (one-dimensional) Maxwell distribution, a Gaussian

$$g(v_z)\sim\exp\left\{-\frac{mv_z^2/2}{k_BT}\right\}, \tag{29}$$

where k_B is Boltzmann's constant and T is the absolute temperature of the sample. The effect of this distribution in velocity is to create a distribution of apparent resonant frequencies ν_0, where the (first-order) Doppler shift gives

$$\nu_0=\nu_{00}(1+v_z/c),\quad \text{so}\quad v_z=\lambda_0(\nu_0-\nu_{00}). \tag{30}$$

Thus the sample effectively contains a whole collection of distinguishable kinds of atoms, with distribution of resonant frequencies

$$g(\nu_0)\sim\exp\left\{-\frac{m}{2k_BT}\,\lambda_0^2(\nu_0-\nu_{00})^2\right\}. \tag{31}$$

Defining the "Doppler width" $\Delta\nu_D$ as the full width at half-maximum of this distribution, we get

$$\Delta\nu_D=\left[\frac{8k_BT\ln 2}{m\lambda_0^2}\right]^{1/2}, \tag{32}$$

and the Doppler distribution, normalized to unit area, becomes

$$g(\nu_0)=\left[\frac{4\ln 2}{\pi\Delta\nu_D^2}\right]^{1/2}\exp\left\{-\ln 2\left(\frac{\nu_0-\nu_{00}}{\Delta\nu_D/2}\right)^2\right\}. \tag{33}$$

The utility of this normalized distribution is that results previously calculated for motionless atoms, all of one resonant frequency ν_0, can be transformed to results applicable to the actual Doppler distribution of atoms by a simple convolution. For example, the previously computed index of refraction $n(\nu;\nu_0)$, a function of frequency ν for a given line center ν_0, changes to

$$n(\nu)=\int_{-\infty}^{\infty}g(\nu_0)\,d\nu_0\;n(\nu;\nu_0). \tag{34}$$

Similar convolutions apply to the attenuation and the Faraday-rotation signals $\beta(\nu)$ and $\Delta\theta(\nu)$. In the limit that the Doppler width $\Delta\nu_D$ is negligible, the distribution function $g(\nu_0)$ turns into the delta function $\delta(\nu_0-\nu_{00})$, and the convolution reproduces the original results. Alternatively, in the limit that the laser frequency's detuning from resonance $\nu-\nu_{00}$ is much larger than either the Doppler width or any Zeeman shift, this delta-function approximation is a good one; thus the Becquerel result derived above remains valid for ordinary nonresonant Faraday rotation. But for the experimental situation described in Sec. III, the case of interest is at the other extreme, with the room-temperature Doppler width exceeding the natural linewidth by a factor of about 100. This has dramatic consequences for the width and size of the absorption, dispersion, and Faraday-rotation signals. The Appendix discusses suitable numerical methods for performing the convolution integrals, but we go on here to present some of the results.

The results easiest to intuit are for absorption. The convolution defined by (34) preserves the total area under the absorption curve, and intuition hints, and computation confirms, that its width will increase from the natural linewidth to very nearly the Doppler width. The consequence is that the absorption at line center must decrease by about the same factor of 100 by which the linewidth increases. Less intuitively obvious are the results for dispersion, though clearly the convolution must smear out the width of the narrow dispersion feature by a similar large factor. Numerical evalua-

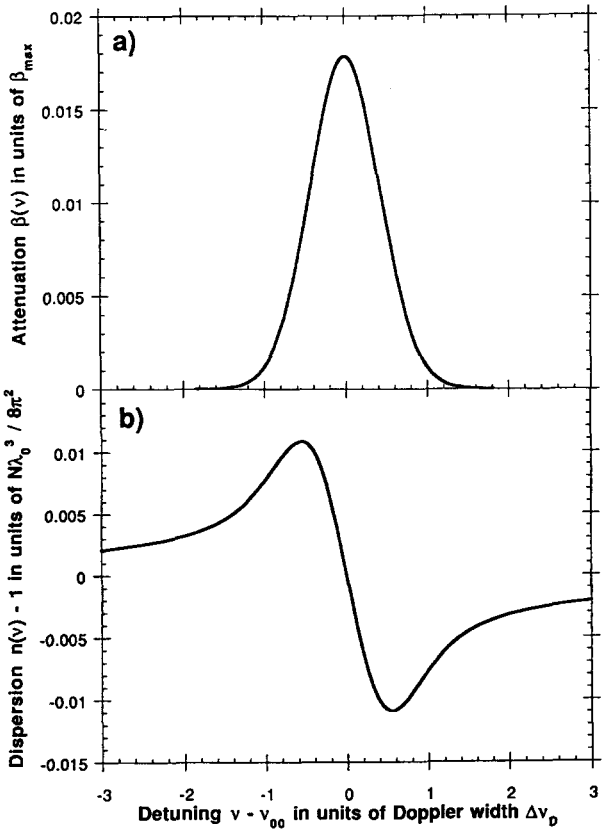

Fig. 4. Graphs of the absorption (a) and dispersion (b) signals computed for the model two-level atomic system, in the presence of Doppler broadening. The curves were computed via (34) and the numerical methods of the Appendix; the horizontal scale is in units of the "Doppler width" $\Delta\nu_D$, and the vertical scales are in the same units as those of Fig. 2. The curves are computed assuming a Doppler width $\Delta\nu_D$ of 511 MHz and a natural linewidth $\Delta\nu$ of 6.24 MHz.

tions confirm this, with the broadened dispersion curve reaching its extrema just outside the frequencies at which the absorption curve reaches its half-maxima. Just as for the absorption curve, so too for the dispersion: this hundredfold increase in width is accompanied by a decrease in height by a similar factor. The results are shown in Fig. 4, which resemble the unbroadened curves of Fig. 2 in character, but which are smaller in vertical scale. Remarkably enough, the dispersion *per unit absorption* is scarcely affected by Doppler broadening; in fact, for a Doppler-broadened sample of density sufficient to give the same absorption at line center, the dispersion (at its extrema) is actually some 23% larger than in the unbroadened case.

Since the Faraday-rotation signal is related to the difference between two dispersion signals, the same results apply to it. The large increase in horizontal scale implies that the magnetic field required to maximize the line-center Faraday rotation will be increased by a similar factor, giving the requirement $kB \approx \Delta\nu_D/2$; for the case of interest, $\Delta\nu_D \approx 500$ MHz, so that a field of about 18 mT (180 Gauss) is required. The previous results for Faraday rotation per unit absorption still apply, with the Doppler-related correction noted above; a sample giving e^{-2} transmission at zero-field line center is predicted to display maximum Faraday rotation of (0.5 rad) $\times(1.23) \approx 35°$.

Finally, Fig. 5 gives some computed results for Faraday rotation as a function of laser frequency, for some different

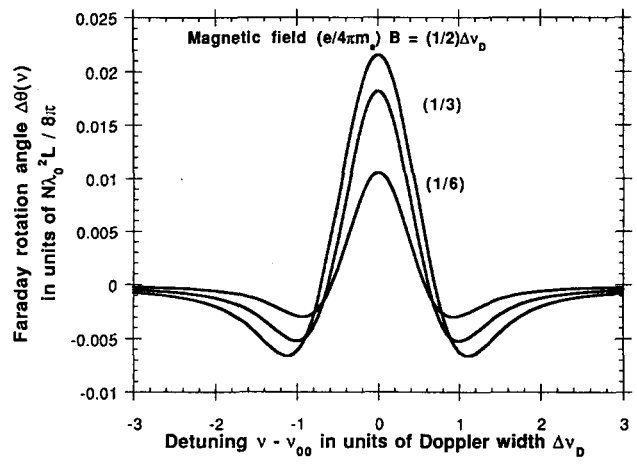

Fig. 5. Faraday rotation angles computed for the model problem of this paper, in the presence of Doppler broadening, for three values of magnetic field strength B: $(e/4\pi m_e)$ $B = \Delta\nu_D/6$, $\Delta\nu_D/3$, and $\Delta\nu_D/2$.

values of magnetic field. Each curve is symmetric around the zero-field line center, and each has long tails of sign opposite to that of the central peak. Since these long tails describe the ordinary off-resonant Faraday rotation, and since Faraday found that the *direction* of off-resonant rotation is the same as that of the (conventional) current in the solenoid producing the field, we deduce that resonant Faraday rotation should have a direction *opposite* to that of the current producing the field; this prediction is readily checked experimentally. Since the Faraday-rotation signal is the difference of two antisymmetric dispersion signals, the Faraday-rotation signals also share their property of having zero net area under their graphs. Thus broadband light cannot be used to display the phenomenon of resonant Faraday rotation; the light interacting with the atoms needs to have a spectral distribution no wider than the Doppler width of the transition.

III. APPARATUS

It is the availability of low power but tunable diode lasers that makes this resonant-Faraday-rotation experiment feasible in the undergraduate laboratory. The diode lasers produced by the millions for compact-disc players have nominal output power 3 mW and wavelength 780 nm; the further facts that their output is of very narrow spectral width (of order 20 to 50 MHz) and also tunable (by changing the diode temperature or injection current) make them wonderfully useful spectroscopic sources. The happy coincidence of their nominal wavelength with the strongest resonance line in the rubidium spectrum, and the extremely convenient vapor pressure of rubidium at room temperature, make diode-laser experiments in rubidium vapor extraordinarily simple and straightforward. Even once-exotic phenomena like Doppler-free spectroscopy via saturated absorption can easily be performed on a benchtop in real time.[16]

The instrumental requirements for diode-laser spectroscopy of rubidium in general can be divided into four categories: laser source, rubidium cell, optical detectors, and ancillary electronics.

For the laser source in such experiments we have used consumer-market laser diodes such as the Mitsubishi ML4102 and Sharp LT022MC devices. Although nominally of 780-nm output wavelength, in fact these devices can be

(discontinuously) temperature tuned at average rate about +0.25 nm/K or −1000 GHz/K, so that diodes of various nominal wavelength can be tuned to near the desired 780-nm wavelength. The nuisance is that these diode lasers exhibit "mode hops" such that any given device has probability below 50% of being tunable to a target wavelength; the easiest solution is to buy and test multiple diodes and find one which does not mode-hop past the desired frequency. In any given mode, these lasers exhibit typical tuning rates of about −120 GHz/K as their case temperature is varied, and −2 GHz/mA as their injection current is varied. In order to vary, and then stabilize, the laser-diode temperature, we have used two-stage thermoelectric servomechanisms,[17] although single-stage systems would likely suffice in this application. In order to perform real-time scanning of the laser frequency, we vary the diode-laser current about its average value of order 60 mA by a sawtooth modulation of audio frequency and peak-to-peak amplitude of about 5 mA; this gives (in addition to a characteristic but undesired modulation of the optical power output) a sawtooth scan of optical frequency over a range of about 10 GHz. This is sufficient to scan over the rubidium resonance line's hyperfine-structure pattern. Finally, since the light emerging from the diode laser is strongly divergent, we use an optimized lens[18] mounted just in front of it to produce a collimated beam of transverse dimensions about 2×5 mm^2. Such a lens can easily be adjusted to produce a beam with a divergence negligible over a meter's flight path; the elliptical cross-section and residual astigmatism common to most diode laser beams do not present a problem in this experiment. However, the large optical intensity of order 5 mW in just a few square millimeters means that optical signals in rubidium can be readily saturated. For experiments such as Doppler-free saturated absorption, this is desirable; but for Faraday-rotation experiments, this can be avoided either by using a less tightly focused laser beam, or by using neutral-density filters to attenuate the laser beam. A suitable level of attenuation is easily found empirically by noting, with decreasing values of laser-beam intensity, an approach to a asymptotic value for the fractional absorption at a rubidium resonance.

The rubidium cell used in such experiments can be of 1- to 3-cm diameter and 5- to 10-cm length; for polarization-sensitive experiments it is very convenient for the cell to have flat end windows at near-normal incidence. Since typical experiments can be done with the rubidium near room temperature, exotic glass is not required. The data below were all obtained with a cell of 25-mm (outside) diameter, 51-mm (inside) length, made of Pyrex glass, and filled with rubidium of natural isotopic abundance, in vacuum (no buffer gas).[19]

The simplest optical detectors for use near 780 nm are silicon photodiodes. These are available in a wide range of shapes and sizes, but all share the remarkably high quantum efficiency (>50%) of silicon p-n photojunctions at these near-infrared wavelengths. The detectors can be operated at zero potential difference, such that they act like ideal current sources, with responsivity of order 0.5 A/W; it is convenient to use operational amplifiers as current-to-voltage converters to generate voltage outputs of order 1 V per milliwatt of incident optical power. Such detector/amplifier combinations can easily have response times under 10 μs, and display output noise equivalent to optical inputs well under 1 μW.

The ancillary electronics needed for this sort of experiment include the servomechanism for diode-laser temperature control, the stable but agile current source of order 0–100 mA, 0–3 V needed to drive the diode laser, and an audio-frequency oscillator to modulate the diode-laser current and thus its output frequency. Remarkably, most of the experiments of interest can be accomplished with signal-capturing electronics no more complicated than a dual-trace oscilloscope; given the laser power and detector noise levels available, even nonlinear optical effects such as saturated absorption can be displayed in real time on an oscilloscope display.

Given such capabilities, only modest additional equipment is needed to perform the Faraday-rotation experiment described here: one needs only a source of magnetic field, and a somewhat more complicated polarization-sensitive optical detector system. The magnetic fields required are of moderate size, up to perhaps 20 mT (200 Gauss), and are easily produced by air-core solenoidal coils. The homogeneity requirements are also easily satisfied, since the fields need to be uniform only over the few-millimeter transverse extent, and the few-centimeter length, of the laser-illuminated rubidium vapor. The data displayed below were obtained using two old short-solenoid coils,[20] each of length 90 mm and effective diameter 112 mm, arranged as an approximate Helmholtz pair. The coils were put in parallel to match the capabilities of an available power supply, and required 41 V at 1.3 A to produce the desired magnetic field. The gap between the coils allowed a Hall-effect Gaussmeter probe to be inserted from the side of the coil, where it could measure the longitudinal field right next to the rubidium cell; alternatively, for a coil system of simpler geometry, the magnetic field could be computed from the measured coil dimensions and current.

The Faraday-rotation experiment clearly requires that the laser light used be linearly polarized upon reaching the sample cell, and that its (rotated) direction of linear polarization be analyzed subsequent to the cell. The input-polarization requirement could be satisfied in many ways, but the simplest is merely to use the intrinsic polarization of the diode-laser emission: for a diode laser at rated power, the nominal polarization purity of >100:1 is easily sufficient for the experiment described here. Thus a linear polarizer suitable for 780 nm (Ref. 21) is only optional; another luxury is a 780-nm half-wave plate, allowing the input polarization to be rotated as desired.

The requirement of detecting the rotation of polarization is a bit more complicated. If the light emerging from the sample cell were purely linearly polarized, then its direction of polarization could be found (at any one wavelength) by searching for extinction with a rotatable linear polarizer used as analyzer. But there are two objections to this classical technique: first, in the presence of differential absorption, the output light is in general elliptically polarized [as (4) shows] so that exact extinction cannot be achieved; and second, this technique does not lend itself to an automated procedure giving a real-time display of polarization-rotation as a function of laser frequency. So for this application we have instead built a simple polarimeter[22] based on a polarizing beamsplitter cube[23] and two photodiodes, arranged as shown in Fig. 6. For input light parallel to the axis shown, and lying in the wavelength range of the device, the beamsplitter approximates very nearly the intended function of transmitting all of the input light of one linear polarization, and deflecting through a right angle all of the input light of the orthogonal linear polarization. In practice, the laser beam used is of

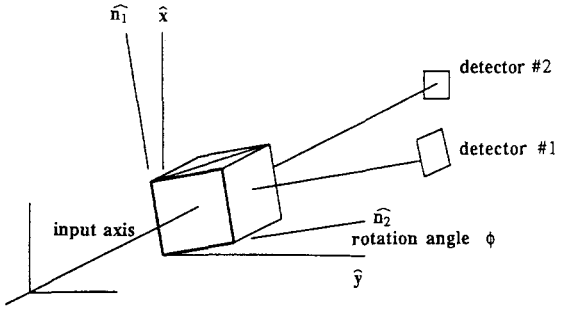

Fig. 6. The polarization analyzer used to gather the Faraday-rotation data of this paper, composed of a polarizing-beamsplitter cube and two detectors arranged to capture the optical power exiting its two output faces. Also displayed are the lab-fixed transverse coordinate axes $\hat{\mathbf{x}}$ and $\hat{\mathbf{y}}$, and the cube-fixed axes $\hat{\mathbf{n}}_1$ and $\hat{\mathbf{n}}_2$.

much smaller transverse, angular, and wavelength extent than the acceptance limits of the beamsplitter, and the two output beams from the beamsplitter are easily captured on modest-area photodiodes.[24] Each photodiode current is separately converted to a voltage,[25] so that two separate real-time voltages, proportional to powers in two orthogonal optical linear polarizations, are simultaneously available for oscilloscope display. The beamsplitter and the two photodiodes are all held together in a cylindrical structure, forming a rigid "analyzer" that can be rotated about a mechanical axis coinciding with the laser beam to be analyzed.

Given a light beam exiting the Faraday medium of the form (4), it is easy to work out the response of the polarization analyzer just described. The simplest case of pure Faraday rotation (with no differential absorption) yields a linearly polarized beam, with polarization axis rotated by angle $\Delta\theta$ from its original x direction. So if in Fig. 6 the analyzer's axes were rotated by $\phi=45°$ away from the $\hat{\mathbf{x}}$ and $\hat{\mathbf{y}}$ directions, it is easy to see that the transmitted and deflected beams would be of equal amplitude in the absence of Faraday rotation; but in the presence of Faraday rotation, one beam would increase, and the other decrease, in amplitude. This is the motivation for taking the difference of the two intensities as the experimental signal. For a general orientation of the analyzer, with the upper face's normal turned through angle ϕ from the x direction, we can define the "eigen-axes" of the beamsplitter to be

$$\hat{\mathbf{n}}_1=\hat{\mathbf{x}}\cos\phi-\hat{\mathbf{y}}\sin\phi,\quad \hat{\mathbf{n}}_2=\hat{\mathbf{x}}\sin\phi+\hat{\mathbf{y}}\cos\phi, \tag{35}$$

in the sense that light of pure linear polarization along $\hat{\mathbf{n}}_1$ will be entirely deflected, and light of pure linear polarization along $\hat{\mathbf{n}}_2$ will be entirely transmitted, by the polarizer. Defining the signal of interest to be the difference in the power emerging from the two faces of the beamsplitter, we have

$$S\equiv P_1-P_2=\frac{1}{2}|\mathbf{E}(L,t)\cdot\hat{\mathbf{n}}_1|^2-\frac{1}{2}|\mathbf{E}(L,t)\cdot\hat{\mathbf{n}}_2|^2. \tag{36}$$

Here, $\mathbf{E}$ is the (complex) electric field incident on the beamsplitter, and we have used the result $|\mathbf{E}|^2/2$ for the time-averaged power of a field written in complex representation. For an electric field of the form (4), the result that emerges is

$$S=2E_0^2\exp[-(\beta_++\beta_-)L]\cos 2(\Delta\theta-\phi), \tag{37}$$

which depends on the same rotation angle $\Delta\theta$ defined in (6), despite the presence of differential absorption ($\beta_+\neq\beta_-$). For the natural choice $\phi=45°$, this simplifies to

$$S=2E_0^2\exp[-(\beta_++\beta_-)L]\sin 2\Delta\theta. \tag{38}$$

This shows that a readily extracted experimental signal is directly related to the sine of twice the Faraday rotation angle $\Delta\theta$ defined by (6). The meaning of the leading coefficient $2E_0^2$ is clearly seen operationally by imagining zero absorption, zero Faraday rotation, and the analyzer set to the $\phi=0°$ or 90° positions, since then (37) gives "baseline signals"

$$S_{\max,\min}=\pm S_0=\pm 2E_0^2. \tag{39}$$

Then, if the analyzer is set to angle $\phi=45°+\epsilon$, one readily finds

$$S=S_0\exp[-(\beta_++\beta_-)L]\sin 2(\Delta\theta-\epsilon), \tag{40}$$

which can be used in three ways. The first application is a method for setting the angle ϕ to the desired 45°: the procedure is to turn off the magnetic field (so that the Faraday rotation $\Delta\theta$ is zero); then the signal S is seen to vanish only when $\sin(-2\epsilon)=0$, i.e., when $\epsilon=0$ or $\phi=45°$. The second application is a method for measuring the Faraday rotation angle $\Delta\theta$ directly: if (for any given laser frequency) the analyzer is turned from the previously established $\phi=45°$ location to that angle at which the observed signal S is driven to zero, then (40) shows that

$$2(\Delta\theta-\epsilon)=0,\quad \text{or}\quad \epsilon=\Delta\theta; \tag{41}$$

i.e., the analyzer has just been turned through exactly the Faraday rotation angle $\Delta\theta$. The third application is a way to get a real-time display related to the instantaneous Faraday rotation as the laser is scanned; this is obtained by rotating the analyzer to $\phi=45°$, by sending voltage signals proportional to P_1 and P_2 to a dual-trace oscilloscope, and by arranging for a vertical deflection proportional to their difference and a horizontal deflection driven by the same low-frequency oscillator that drives the frequency sweep of the laser.

IV. DATA AND DISCUSSION

We turn now to data derived from diode-laser spectroscopy of rubidium vapor, and a discussion of it in terms of the model so far developed.

For purposes of orientation, it is important first to acquire simple absorption data; this can be easily done with the apparatus described above by turning the magnetic field off and by orienting the polarization analyzer (to the $\phi=0$ position) so that the incoming linearly polarized light is entirely transmitted to one of the two photodetectors. Then the intensity of the transmitted light, as a function of laser-diode current, exhibits a graph like that of Fig. 7. This graph, and those to follow, was obtained by operating the diode laser with a sum of a fixed dc, and a sawtooth-modulated ac, injection current. Increasing current is to the right; the diode laser responds to greater current by exhibiting greater output power, and larger output wavelength. The increasing output power is displayed in the linearly rising signal in the figure; the increasing wavelength, or decreasing optical frequency, is chosen to scan over the rubidium D_2 resonance line at 780 nm. The upsloping optical signal (interpolated through the narrow absorption features displayed) is exactly the signal S_0 defined above, since it is obtained for polarimeter angle $\phi=0°$, for no absorption, and for zero magnetic field; knowledge of S_0, and its (unintended) variation with laser frequency, allows a theoretical model to include laser power variation. Of course,

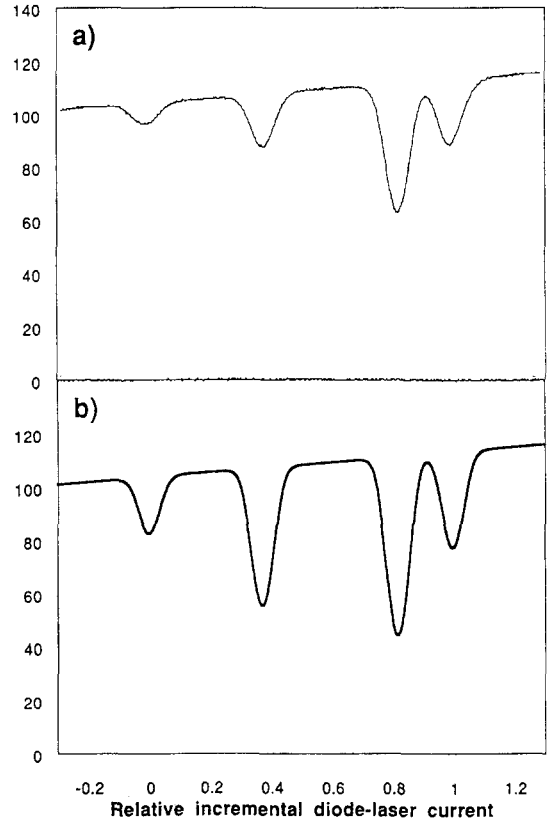

Fig. 7. (a) Intensity of (linearly polarized) light transmitted though a cell of rubidium vapor, as a function of relative incremental current in the diode-laser light source. The central value of diode-laser current has been empirically selected to give a central optical frequency near 384 200 GHz, and the width of the sweep has been selected to give a scan of about 10 GHz in optical frequency. Optical frequency *decreases* to the right; cell length $L=51$ mm, temperature=298 K; magnetic field zero. (b) Theory for this transmission signal, computed using the model described in the text. The horizontal scale, and the size and slope of the baseline, have been adjusted to match the data, but the shapes and sizes of the absorption dips are calculated from, not fit to, the model.

the more interesting content of the data of Fig. 7 is the set of narrow absorption features displayed; this is a high-resolution view of the Rb D_2 line. The scan was taken at low enough intensity (<0.4 mW in a spot about 3×6 mm^2) to avoid the saturation of the absorption features; the scan duration was under 2 ms.

The very first conclusion to be drawn is that rubidium is not as simple as the model introduced so far, since the data show not one, but rather four absorption dips. The structure observed is readily explained in terms of the actual structure of the rubidium D_2 line. This line arises from the $5s\ ^2S_{1/2}-5p\ ^2P_{3/2}$ transition out of the ground state; the combination of the isotopic composition of natural rubidium, and the hyperfine structure of the states involved, give rise to the lines displayed. The two inner lines arise from the 72.15% abundant ^{85}Rb isotope, and the outer ones from the 27.85% abundant ^{87}Rb isotope. The two inner lines are separated by about 3.6 GHz, the ^{85}Rb ground-state hyperfine splitting; similarly the outer lines are separated by about 6.8 GHz. For the purposes of this paper, these splittings can be taken as well known,[26] and they serve as a convenient way to calibrate the optical frequency scale. Each of the four observed absorption dips is broadened by two mechanisms: common to all is the room-temperature Doppler broadening of about 0.51 GHz, and different for each is the (unresolved) upper-state hyperfine structure, which ranges from 0.09 to 0.42 GHz for the various lines.

Clearly, enough is known about rubidium to permit a complete quantum-mechanical calculation of absorption, dispersion, and Faraday rotation;[27] such calculations are simplified by the cylindrical symmetry of the problem, which leaves the magnetic quantum number m_F a good quantum number even in the presence of the magnetic field, and which preserves the selection rules of $\Delta m_F=\pm 1$ for the fields described by $\mathbf{E}_\pm$. But such exact calculations are not particularly illuminating, and for the purposes of this paper we will instead "adapt reality to the model" by the following prescription. We will treat not only the two isotopes, but also the two ground-state hyperfine populations of each isotope, as separate noninteracting populations; we will ignore the upper-state hyperfine structure entirely; and we will assume that the transitions out of the ground state obeying the $\Delta m_F=\pm 1$ selection rules follow a simple Zeeman shift given by (13). In other words, we will treat the data as if rubidium were a mixture of four distinguishable kinds of the model atoms treated in the theory section above; the expected relative populations of the four "species" are given in Table I.

With this heavy-handed approximation, we can readily predict the expected size of the absorption signals; using the number densities of Table I for each of the four notional species of rubidium, we can use (15) to evaluate the absorption exponents $2\beta(\nu)L$ for the four species present, and then subject these to Doppler broadening by the methods of the

Table I. Statistical weights and number densities for the four "species" of rubidium giving rise to the four absorption features in Fig. 7. The features are labeled by the convention of Ref. 26, and are given in order of decreasing optical frequency.

Feature	Isotope and F value	Isotopic abundance	Statistical weight[a]	Overall weight	Number density[b]
(iv)	^{87}Rb, $F=1$	0.2785	3/8	0.1044	0.26×10^{16}
(iii)	^{85}Rb, $F=2$	0.7215	5/12	0.3006	0.75×10^{16}
(ii)	^{85}Rb, $F=3$	0.7215	7/12	0.4209	1.05×10^{16}
(i)	^{87}Rb, $F=2$	0.2785	5/8	0.1741	0.44×10^{16}

[a]Statistical weight is computed from $(2F+1)/2(2I+1)$, where $2F+1$ is the number of degenerate magnetic sublevels in a ground-state hyperfine level of a given F value, and $2(2I+1)$ is the total number of ground-state sublevels.

[b]Number densities (in m^{-3}) are computed assuming rubidium temperature $T=25$ °C=298 K, and overall rubidium number density 2.5×10^{16} m^{-3} (from Ref. 12).

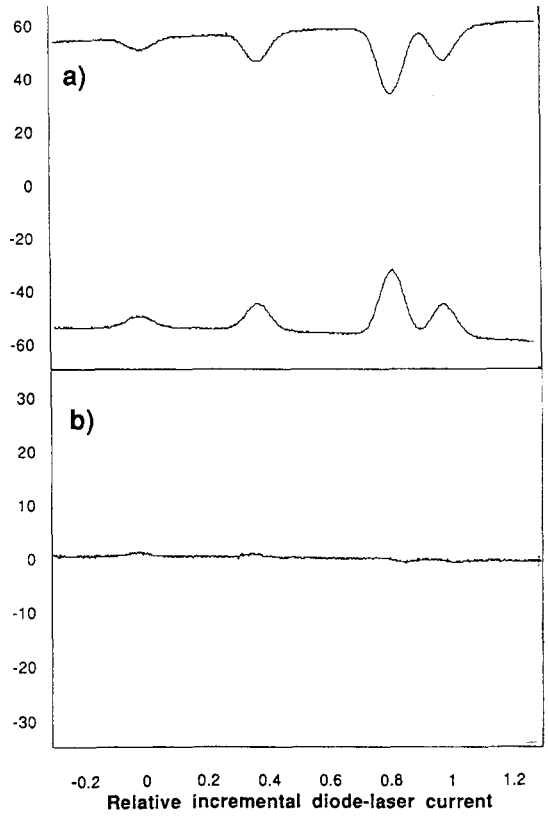

Fig. 8. (a) The signals obtained from the two photodetectors of the polarization analyzer of Fig. 6, under conditions of polarizer angle $\phi=45°$, zero magnetic field, and one signal electronically inverted. (b) The sum of the two signals of (a), further expanded vertically by a factor of 2; this is the signal representing zero Faraday rotation.

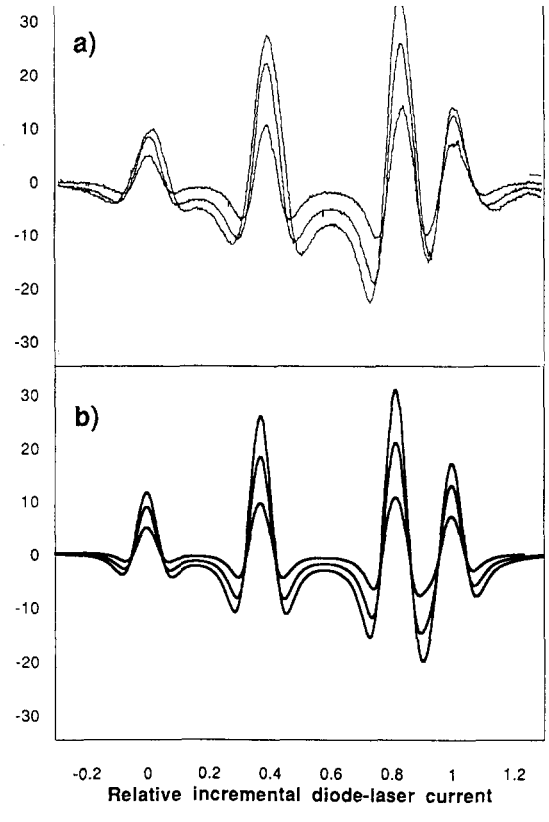

Fig. 9. (a) The experimental Faraday-rotation signal for three values of magnetic field strength ($B=5$, 10, and 15 mT), obtained at the same scale as the "baseline" data of Fig. 8(b). (b) Theoretical Faraday-rotation signals expected for this experimental situation, computed using the model described in the text. The theory uses the same horizontal and vertical scaling as in Fig. 7(b), and no adjustable parameters.

Appendix. Summing these and using the $B=0$, $\Delta\theta=\phi=0$ version of (37) above then gives a theoretical model for the absorption signal predicted for the sample. Figure 7(b) shows the results, where the horizontal axis, and the vertical scale and baseline slope, have been scaled to match the data, but in which no other parameters are adjusted. Comparing the data and the model, we see fine agreement in the shape of the absorption signals, showing that the computed Doppler broadening is really being observed; but the agreement in absolute and relative intensities is not so good. This may perhaps be attributed to optical pumping of the sample; though the light intensity is low enough to avoid saturation (depletion of the ground-state population), it may not be low enough to avoid optical pumping (redistribution of the ground-state magnetic sublevels' population).

Now there are only two experimental changes needed to display Faraday rotation with this system. The first is to rotate the polarization analyzer to the $\phi=45°$ position, to view the signals from both photodetectors, to invert one of them, and to display both on a dual-trace oscilloscope. The resulting displays are shown in Fig. 8, where the two signals are shown before and after algebraic addition on the 'scope. As expected, the two separate signals are nearly identical, and the sum signal is nearly zero, on the 'scope. The second change is to raise the magnetic field from its previous zero value to a succession of fixed values. The results for the previously vanishing "sum signal" on the 'scope are displayed in Fig. 9(a), for which the 'scope gain is the same as it was in Fig. 8(b). Each of the traces displays a set of four signals, each arising at the location of one of the four zero-field absorption features; each of the four signals resembles the symmetric resonant-Faraday-rotation signals predicted by theory and depicted in Fig. 5. Each of these traces was obtained in one single sweep of total duration less than 2 ms, so the Faraday rotation thus displayed is truly a real-time phenomenon; in fact the inductive time constant of the magnetic-field coils is the factor limiting the rate at which the Faraday-effect display on the oscilloscope can be changed!

For purposes of more detailed comparison with the theory, the theoretical prediction (40) was evaluated under the following assumptions: The leading factor S_0 (representing the characteristic variation in intensity that accompanies a diode laser's tuning) was taken from the pure absorption data above; the attenuation constants β_+ and β_- were taken from Doppler-broadened and Zeeman-shifted versions of (15), and the Faraday rotation angle $\Delta\theta$ was taken from the Doppler-broadened version of (21). This was done for four features, assumed to be located at the positions of the four zero-field absorption phenomena, and assumed to arise from species of the number densities given in Table I. Again, the quantities $(\beta_+ + \beta_-)$ and $\Delta\theta$ in (40) are linear in number density N, so they can be summed over the assumed four species to give values applicable to the whole sample; then evaluating the exponential and sine functions in (40) gives a result comparable to the data. The results are shown in Fig. 9(b), which displays a set of theoretical simulations of the actual experi-

ment. There are no new parameters adjusted in computing the Faraday signal, since the scaling of Fig. 7 suffices to fix all the necessary quantities. The agreement of the two halves of Fig. 9 illustrates that a simple model of atomic dispersion is indeed sufficient for a detailed description of resonant Faraday rotation; there is surprisingly good agreement in the details of the vertical scale of the signals, and some disagreement in the details of the broadening and saturation of the Faraday rotation signals with increasing magnetic field.

V. CONCLUSIONS AND APPLICATIONS

We have shown that the Faraday effect is readily detected in a diode-laser experiment in rubidium vapor, and that it has both an unusually large size and a particularly interesting structure in the immediate vicinity of the D_2 resonance line. We have also shown that a relatively simple theory can describe most of the features of the resonant structure, and this illustrates the intimate connection between absorption and dispersion in this resonant interaction of light and matter.

It is worth contemplating how the theoretical and experimental work discussed in this paper could be extended. An obvious extension to the theory would be to replace the simple atomic model used above with a quantum-mechanical model of actual rubidium, complete with the hyperfine structure of both the ground and excited states, and the correct magnetic-field dependence of all the energy levels. This has been done for the analogous D_2 line in cesium (in connection with experiments in parity violation),[28] and affords a useful exercise in matrix diagonalization. This, however, would still not give a perfect description of the experiment, since at easily accessible levels of laser intensity there arise nonlinear effects such as optical pumping, saturation, and velocity redistribution.[29]

On the experimental side, one could imagine a Doppler-free Faraday-effect experiment, using a "pump beam" to isolate one velocity class, and a "probe beam" passing through the same sample to measure Faraday rotation. Such an experimental arrangement would represent the use of the method of polarization spectroscopy[30] in the presence of a magnetic field. With the limitation of Doppler broadening removed, the next obstacle to spectroscopic resolution would be the intrinsic linewidth of free-running laser diodes. This limit could in turn be surpassed through the use of extended-cavity diode-laser systems of very narrow spectral widths; this would leave the natural linewidth of rubidium transitions as the limit on spectroscopic resolution.

There are other experimental arrangements that could be tried; much higher rubidium densities are easily accessible at moderately elevated temperatures. A larger departure would be investigation of the Voigt effect, the study of polarization rotation using a magnetic field transverse (rather than parallel) to the direction of light propagation.[31]

It is also worth remarking on a fascinating technological application of the Faraday effect for producing optical filters of extremely narrow bandwidth, but high peak transmission and wide field of view. The simplest of such filters is a sandwich with a rather high-density vapor cell between a pair of crossed linear polarizers. Such a filter would be opaque at all wavelengths in the absence of a magnetic field; in the presence of a suitable field, it is still opaque far from a resonance line (since the Faraday rotation is very small at large detuning) and right near a resonance line (since absorption in the vapor is very large there). But because absorption drops off with detuning more rapidly than does the Faraday-rotation signal, it is possible for the cell to offer small absorption at two points on either side of the resonance where Faraday rotation is still as large as 90°. The result is that the sandwich becomes nearly transparent to light in two spectral regions each only a few GHz wide; this represents a passband whose width is only a few parts per million of the optical frequency. Filters like these have been proposed for systems involving laser communication with submerged submarines.[32]

ACKNOWLEDGMENTS

The development of this experiment was supported, in part, by National Science Foundation Grant No. DUE-9255528, and thanks are also due to the participants in the diode-laser workshop thereby supported for their comments on the experiment. I also thank Hugh Robinson for helpful discussions about this paper, and Leo Hollberg for the hospitality that enabled me to write it.

APPENDIX

The presence of Doppler broadening leads to the need to evaluate convolution integrals of the form

$$\int_{-\infty}^{\infty} g(\nu_0)\,d\nu_0\,\frac{(\Delta\nu/2)\ \text{or}\ (\nu_0-\nu)}{(\nu_0-\nu)^2+(\Delta\nu/2)^2}$$

for absorption and dispersion signals, respectively, where $g(\nu_0)$ is the normalized Gaussian function defined by (33). The further case of the Faraday-rotation signal can be handled as a difference of two dispersion signals with distinct line centers. The Doppler broadening of Lorentzian absorption signals leads to the well-known "Voigt profile," and a recent article[33] describes various methods for computing these. Given the need to compute the broadening of both absorption and dispersion signals, and given modern computational environments, the best route to a solution seems to be via the complex error function.

The change of variable

$$t=\frac{2\sqrt{\ln 2}}{\Delta\nu_D}(\nu_0-\nu_{00})$$

transforms the integral above into the standard form

$$\frac{1}{\sqrt{\pi}}\int_{-\infty}^{\infty}\exp(-t^2)dt \times\frac{(\Delta\nu/2)\ \text{or}\ [\nu_{00}+(\Delta\nu_D/2\sqrt{\ln 2})t-\nu]}{[\nu-\nu_{00}-(\Delta\nu_D/2\sqrt{\ln 2})t]^2+(\Delta\nu/2)^2}$$

$$=\frac{2}{\Delta\nu_D}\sqrt{\frac{\ln 2}{\pi}}\int_{-\infty}^{\infty}e^{-t^2}\,dt\,\frac{y\ \text{or}\ (t-x)}{(x-t)^2+(y)^2},$$

where

$$x=\frac{2\sqrt{\ln 2}}{\Delta\nu_D}(\nu-\nu_{00})\quad\text{and}\quad y=\frac{2\sqrt{\ln 2}}{\Delta\nu_D}\frac{\Delta\nu}{2}.$$

Integrals of this form lack antiderivatives, but are related to the "complex error function" $w(z)$ defined[34] by

$$w(z)=\exp(-z^2)\operatorname{erfc}(-iz)=\exp(-z^2)[1-\operatorname{erf}(-iz)].$$

In fact the latest integral above is given very simply by[35]

$$\int_{-\infty}^{\infty} e^{-t^2}\,dt\,\frac{y \text{ or } (t-x)}{(x-t)^2+(y)^2}$$

$$=\pi\{\text{Re } w(x+iy) \text{ or } -\text{Im } w(x+iy)\}.$$

Since the complex function $w(z)$, or at least erf(z), is available as a library function in some modern numerical analysis packages, and since the real and imaginary parts of $w(z)$ simultaneously provide the broadening of the absorption and dispersion lineshapes respectively, this computational method has been used to generate the signals required in this paper. In the case of interest, the y parameter has the fixed and small value of about 0.0102, and the x parameter reaches about ± 33 for detuning $\nu-\nu_{00}$ of ± 10 GHz.

[1]Michael Faraday, *Experimental Researches in Electricity*, paragraphs 2146–2242 [in Vol. III of the reprint edition (Dover, New York, 1965)].

[2]E. Scott Barr, "Men and milestones in optics. V: Michael Faraday," Appl. Opt. **6**, 631–637 (1967).

[3]E. D. Palik and B. W. Henvis, "A bibliography of magnetooptics of solids," Appl. Opt. **6**, 603–630 (1967).

[4]D. Macaluso and O. M. Corbino, "On a new effect on light traversing certain metallic vapors in a magnetic field," C. R. Acad. Sci. **127**, 548 (1898).

[5]Pochi Yeh, "Dispersive magnetooptic filters," Appl. Opt. **21**, 2069–2075 (1982).

[6]Frank J. Loeffler, "A Faraday rotation experiment for the undergraduate physics laboratory," Am. J. Phys. **51**, 661–663 (1983).

[7]Frank L. Pedrotti and Peter Bandettini, "Faraday rotation in the undergraduate advanced laboratory," Am. J. Phys. **58**, 542–545 (1990).

[8]L. J. Aplet and J. W. Carson, "A Faraday effect optical isolator," Appl. Opt. **3**, 544–545 (1964).

[9]Daryl W. Preston and Eric R. Dietz, *The Art of Experimental Physics* (Wiley, New York, 1991), pp. 355–366.

[10]This labeling avoids the troublesome and contradictory conventions associated with right- and left-handed circular polarizations.

[11]Amnon Yariv, *Optical Electronics* (HRW, New York, 1985), 3rd ed., Chap. 5; this result omits the "counter-rotating" term, so it is valid anywhere near resonance, but not at "dc."

[12]A. M. van der Spek, J. J. L. Mulders, and L. W. G. Steenhuysen, "Vapor pressure of rubidium between 250 and 298 K determined by combined fluorescence and absorption measurements," J. Opt. Soc. Am. B **5**, 1478–1483 (1988).

[13]H. Becquerel, "On an explanation applicable to the phenomena of Faraday and Zeeman," C. R. Acad. Sci. **125**, 679 (1897).

[14]Jan Evetts (Ed.). *Concise Encyclopedia of Magnetic & Superconducting Materials* (Pergamon, New York, 1992), article on Magnetooptics.

[15]Robert W. Schmieder, Allen Lurio, W. Happer, and A. Khadjavi, "Level-crossing measurement of lifetime and hfs constants of the $^2P_{3/2}$ states of the stable alkali atoms," Phys. Rev. A **2**, 1216–1228 (1970).

[16]John R. Brandenberger, *Lasers and Modern Optics in Undergraduate Physics* (Lawrence University, Appleton, WI, 1989), pp. 33–58.

[17]D. A. Van Baak, "Temperature servomechanisms using thermoelectric modules," Am. J. Phys. **60**, 803–815 (1992).

[18]Lens LP-04 by Universe Kogaku (Glen Cove, NY).

[19]Cell supplied by Opthos, Inc. (Rockville, MD).

[20]Coils (Heath #40-694) from the Berkeley Physics course.

[21]Note that the polarizing efficiency of conventional Polaroid sheets is very low at these wavelengths.

[22]H. Adams, D. Reinert, P. Kalkert, and W. Urban, "A differential detection scheme for Faraday rotation spectroscopy with a color center laser," Appl. Phys. B **34**, 179–185 (1984).

[23]Polarizing beamsplitter 03 PBS 065 by Melles-Griot (Irvine, CA).

[24]Photodiodes VTB-6061 from EG&G Vactec (St. Louis, MO).

[25]Using dual op-amp LM833 from National Semiconductor, with feedback resistors of 3.9 kΩ (and parallel capacitors of 220 pF for high-frequency roll-off).

[26]G. P. Barwood, P. Gill, and W. R. C. Rowley, "Frequency measurements on optically narrowed Rb-stabilized laser diodes at 780 nm and 795 nm," Appl. Phys. B **53**, 142–147 (1991).

[27]Z. Wu, M. Kitano, W. Happer, M. Hou, and J. Daniels, "Optical determination of alkali metal vapor number density using Faraday rotation," Appl. Opt. **25**, 4483–4492 (1986). In this paper it is shown that an exact treatment gives a Faraday rotation (far from resonance) larger, by a factor of 7/6, than the one computed using the simple model described here.

[28]X. Chen, V. L. Telegdi, and A. Weis, "Magneto-optical rotation near the cesium D_2 line (Macaluso-Corbino effect) in intermediate fields: I. Linear regime," J. Phys. B **20**, 5653–5662 (1987).

[29]S. I. Kanorsky, A. Weis, J. Wurster, and T. W. Hänsch, "Quantitative investigation of the resonant nonlinear Faraday effect under conditions of optical hyperfine pumping," Phys. Rev. A **47**, 1220–1226 (1993).

[30]C. Wieman and T. W. Hänsch, "Doppler-free laser polarization spectroscopy," Phys. Rev. Lett. **36**, 1170–1173 (1976).

[31]Kazuyuki Muroo, Takeshi Matsunobe, Yukio Shishido, Yoshitaka Tukubo, and Manabu Yamamoto, "Resonant Voigt-effect spectrum of the rubidium D_2 transition," J. Opt. Soc. Am. B **11**, 409–414 (1994).

[32]Yat Ching Chan and Jerry A. Gelbwachs, "A Fraunhofer-Wavelength Magnetooptic Atomic Filter at 422.7 nm," IEEE J. Quant. Elec. **29**, 2379–2384 (1993).

[33]William J. Thompson, "Numerous neat algorithms for the Voigt profile function," Comput. Phys. **7**, 627–631 (1993).

[34]Milton Abramowitz and Irene K. Stegun, *Handbook of Mathematical Functions* (NBS, Washington, DC, 1964), 7.1.3.

[35]Reference 34, 7.4.13 and 14.

THE SAME OLD STUFF, YEAR AFTER YEAR

Instead of teaching the same old stuff year after year, [the teacher] will constantly enrich his knowledge, keep his teaching alive and dynamic, and prevent his mind from falling into the disease of authority and age, which is paralysis.

There is no other solution. Life is a process of constant change. No one can teach a subject in the same way two years running. Even if he uses the same books and teaches the same facts and conclusions, the second year he will have blurred a few outlines by repetition, cut a few corners because of age. The alternatives are only these: to allow your teaching to petrify by neglect, or constantly to refresh it by transfusions of new vitality and interest from your own reading. The choice is not too difficult, if it is clearly seen. One of the few consolations of age is that, while the body becomes weaker, the mind can grow stronger and richer.

Gilbert Highet, *The Art of Teaching* (Vintage Books, New York, 1989; originally published by Alfred A. Knopf, 1950), pp. 83–84.